

Noise and ac-dc interference phenomena in the charge-density-wave conductor $K_{0.3}MoO_3$

M. F. Hundley* and A. Zettl

Department of Physics, University of California at Berkeley, Berkeley, California 94720

(Received 7 January 1988; revised manuscript received 28 October 1988)

We demonstrate that extremely thin ($< 1 \mu\text{m}$ thick) samples of the charge-density-wave (CDW) conductor $K_{0.3}MoO_3$ display high-quality narrow-band noise spectra when driven by a dc electric field. In the presence of combined dc and large-amplitude ac fields, the CDW becomes mode locked to the external signal, giving rise to Shapiro steps in the dc I - V characteristics. In the presence of combined dc and small-amplitude ac fields, distinct resonance features in the complex ac conductivity $\sigma(\omega)$ are observed whenever the internal and external frequencies coincide. Analysis of the Shapiro-step interference suggests that the ac-dc interference arises from a direct coupling between the driving fields and the low-frequency dielectric relaxation mode in $K_{0.3}MoO_3$. Resonances in the ac conductivity are shown to be analogous to those present in a phase-shifted resonant harmonic oscillator. Both noise and interference experiments yield a ratio between the narrow-band noise frequency and the CDW current-density of $f_{\text{NBN}}/J_{\text{CDW}} = 12 \pm 3 \text{ kHz cm}^2/\text{A}$, suggesting that the intrinsic pinning potential in $K_{0.3}MoO_3$ has a periodicity equal to the CDW wavelength.

I. INTRODUCTION

The study of the dynamical properties of the sliding-charge-density-wave (CDW) state in quasi-one-dimensional materials began in 1976 when Monceau *et al.* first discovered that the CDW in $NbSe_3$ could be depinned by applying a small dc electric field along the crystal chain axis.¹ Since this initial discovery, a great deal of work has been performed by many researchers in an attempt to understand the transport properties of the dynamic CDW state.² One of the most intriguing properties associated with CDW conduction is that of the so-called narrow-band-noise (NBN) oscillations which accompany the dc motion of a sliding CDW. NBN oscillations have been observed in all sliding CDW conductors.² The fundamental NBN frequency f_{NBN} directly scales with the charge-density-wave current density J_{CDW} :³

$$J_{\text{CDW}} = a f_{\text{NBN}}, \quad (1)$$

where a is a sample- and temperature-dependent constant. Although debate⁴ continues, there is much evidence to suggest that the NBN oscillations are a bulk phenomenon, possibly originating from the CDW's interaction with the potential provided by pinning impurities.⁵

A number of unusual interference effects occur^{6,7} in a charge-density-wave material when it is driven by combined ac and dc driving fields of the form

$$V = V_{\text{dc}} + V_{\text{ac}} \cos(\omega t). \quad (2)$$

The effects reflect a direct interaction between the depinned CDW oscillating at a frequency f_{NBN} and the external fields oscillating at a frequency $\omega/2\pi$.

For values of V_{ac} comparable to or larger than the CDW depinning threshold voltage V_T , the CDW can become *mode locked* to the external signal over an appreciable range of dc bias voltage.

This results in the formation of so-called Shapiro steps in the current-voltage (I - V) characteristics of the sample; the steps also appear in the sample's differential resistance.⁶⁻⁸ Shapiro-step interference occurs whenever the externally applied frequency $\omega/2\pi$ is related to the internal NBN frequency f_{NBN} by

$$p \frac{\omega}{2\pi} = q f_{\text{NBN}}, \quad (3)$$

where p and q are integers.⁹ The index n of a specific step is defined as $n = p/q$. For integer values of n , the Shapiro step forms due to the interaction between the NBN fundamental f_{NBN} ($q=1$) and the n th harmonic of the external signal; this is referred to as a harmonic Shapiro step. For noninteger values of n , the Shapiro step is referred to as a subharmonic step. Shapiro steps have been extensively studied in $NbSe_3$,⁶⁻¹⁰ and to a lesser extent in TaS_3 .¹¹

For small values of V_{ac} ($V_{\text{ac}} \ll V_T$) mode locking of the entire CDW condensate does not readily occur. Nonetheless, the sample ac conductivity is strongly affected by interference between the internal and external frequencies. The complex ac conductivity $\sigma(\omega)$ is determined by measuring the in-phase and out-of-phase response of the sample at the frequency $\omega/2\pi$ when a driving field of the form given by Eq. (2) is applied, with $V_{\text{ac}} \ll V_T$. As the test frequency $\omega/2\pi$ or the dc bias V_{dc} is swept, interference in $\sigma(\omega)$ occurs when the conditions of Eq. (3) are satisfied. Whenever $\omega/2\pi = f_{\text{NBN}}$, a dramatic "inductive" resonance occurs; this effect has been studied extensively in highly coherent $NbSe_3$ (Refs. 7 and 10) and less extensively in $K_{0.3}MoO_3$.¹²

$K_{0.3}MoO_3$ (potassium blue bronze) undergoes a Peierls transition at $T_P = 180 \text{ K}$ which gives rise to the formation of a depinnable incommensurate CDW.¹³ In addition to

displaying nonlinear conductivity and NBN, this material also exhibits a low-frequency (< 10 MHz) dielectric relaxation mode whose characteristic frequency is highly temperature dependent.^{14,15} The mechanisms responsible for the creation of this mode are thought to be closely related to those which cause many metastable effects.¹⁶ In the microwave region (> 100 MHz), $K_{0.3}MoO_3$ also exhibits a conductivity mode analogous to that seen in other CDW materials.¹⁷

Usually, $K_{0.3}MoO_3$ samples display very weak NBN spectra, indicating that the sliding state in this material is generally very incoherent.¹³ In contrast, the semimetallic CDW material $NbSe_3$ shows highly coherent behavior. Samples of these two materials are usually very different in size. $NbSe_3$ grows in fine needlelike whiskers with typical dimensions of $1\text{ mm} \times 5\text{ }\mu\text{m} \times 1\text{ }\mu\text{m}$ (volume of $5 \times 10^{-9}\text{ cm}^3$), whereas blue-bronze samples are far larger, with typical dimensions of $1 \times 0.5 \times 0.25\text{ mm}^3$ (volume of $1.25 \times 10^{-4}\text{ cm}^3$). Hence, a typical blue-bronze sample which displays weak NBN is also 5 orders of magnitude larger in volume than a typical highly coherent $NbSe_3$ crystal. This suggests that NBN generation is, in general, a finite-size effect in CDW materials, as has been suggested for $NbSe_3$.⁵ For this reason, we have examined extremely thin samples of $K_{0.3}MoO_3$, with typical volumes of 10^{-8} – 10^{-7} cm^3 , in order to observe strong CDW coherence effects. We find that these samples do indeed display a highly coherent dynamic CDW response.

Our extremely thin, optically transparent single crystals of $K_{0.3}MoO_3$ display NBN spectra of exceptional quality. When examined in the presence of combined ac and dc driving fields, the crystals exhibit both strong mode locking in differential resistance (dV/dI) traces and large resonance anomalies in the complex frequency-dependent conductivity. We have measured the Shapiro-step spectrum as a function of both applied ac amplitude and frequency (10–100 kHz), and find reasonable agreement between the data and a simplified classical single-particle CDW equation of motion.¹⁸ The analysis suggests that the external fields couple to the *low-frequency dielectric relaxation mode*¹⁴ rather than to the high-frequency pinned-phason mode. We have also investigated the ac-dc interference effects on the complex ac conductivity $\sigma(\omega)$ ($\omega/2\pi < 1$ MHz). Large and narrow inductive dips occur when the external frequency equals the narrow-band-noise frequency. We show that this resonance phenomenon appears analogous to that present in the response of a phase-shifted resonant harmonic oscillator. The highly coherent response of the samples examined in this study provides a means of accurately measuring the CDW-current-density-to-NBN-frequency ratio; we find that the empirically determined value implies a pinning-potential periodicity equal to the CDW wavelength.¹⁹

The remainder of this paper is organized as follows. A description of both sample-preparation techniques and experimental methods are presented in Sec. II. Experimental results are given in Sec. III, followed by an analysis in Sec. IV. Lastly, we briefly summarize our findings and present concluding remarks in Sec. V.

II. SAMPLE PREPARATION AND EXPERIMENTAL TECHNIQUES

Single crystals of $K_{0.3}MoO_3$ were obtained using an electrochemical growth technique²⁰ which produces high-quality crystals with typical dimensions of $2 \times 1 \times 1\text{ mm}^3$. The thin, optically transparent samples were prepared by first cleaving a large crystal down to a thickness of roughly $200\text{ }\mu\text{m}$. The cleaved face was then glued to a sapphire substrate with a cryanoacrylic adhesive ("super glue"). The mounted crystal was then cleaved still further using the "Scotch tape" method, until a transparent piece was obtained. By following this procedure, we have been able to obtain samples with uniform thicknesses ranging from 0.1 to $1\text{ }\mu\text{m}$ and areas of up to 1 mm^2 . The sample used to study ac-dc interference effects in blue bronze was determined to be $0.2\text{ }\mu\text{m}$ thick by using a Tencor Instruments step-height analyzer; the sample's complete dimensions were $0.625\text{ mm} \times 0.5\text{ mm} \times 0.2\text{ }\mu\text{m}$ (volume of $6.25 \times 10^{-8}\text{ cm}^3$), with the b axis directed along the largest dimension. Electrical contacts were made to this sample via evaporated indium pads and silver conducting paint. The two-probe room-temperature (RT) resistivity was found to be $\rho_{RT} = 3.5 \times 10^{-4}\text{ }\Omega\text{ cm}$. All measurements presented in this paper were made by using a two-probe current-driven configuration. For comparative purposes, all data presented in this paper are from the same $K_{0.3}MoO_3$ sample. We have obtained qualitatively similar results on all submicrometer blue-bronze samples that we have examined.

Current-driven narrow-band-noise spectra were measured with a Hewlett-Packard 8558B spectrum analyzer. Shapiro steps were obtained by simultaneously driving the sample with both a dc and an ac ($\omega/2\pi = 10$ – 100 kHz) current. The differential resistance dV/dI was measured via a low-frequency bridge with lock-in detection of a low-frequency (280 Hz) modulation signal.

The complex ac conductivity $\sigma(\omega)$ (both frequency and dc-bias dependent) was measured at frequencies between 100 Hz and 1 MHz by a computer-controlled Hewlett-Packard 4192A impedance analyzer. The ac amplitude was always kept well below the CDW depinning voltage, so that the ac signal would act only as a probe of the sample's conductivity. The evaporated indium contacts were found to be of high quality by analyzing the sample response in the complex impedance plane.¹⁴

Our experiments were performed at 77 K to facilitate a comparison of the data with other previously published results. The extremely fragile crystals were slowly cooled in a helium-gas-flow system to prevent fracturing them during the cool-down process. The helium-gas-flow system also provided stable temperature control.

III. EXPERIMENTAL RESULTS

The NBN spectrum produced by a $0.2\text{-}\mu\text{m}$ -thick blue-bronze specimen at 77 K is presented in Fig. 1. The spectrum exhibits a sharp fundamental at $f_{\text{NBN}} = 70\text{ kHz}$, as well as four higher harmonics at 140 , 220 , 280 , and 360 kHz . This sharp spectrum indicates that the sliding CDW state is very coherent. The quality of this NBN

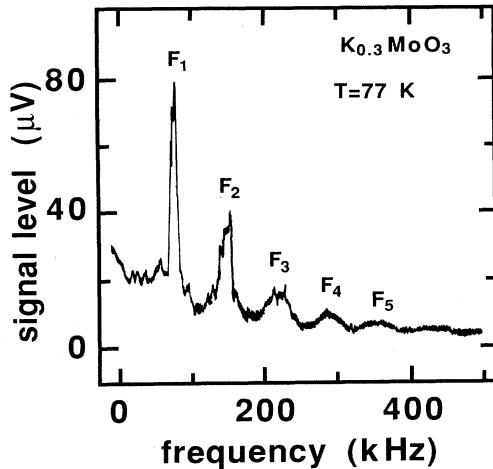


FIG. 1. Narrow-band noise spectrum from a thin sample of $K_{0.3}MoO_3$ at $T=77$ K.

spectrum exceeds that of those published previously,^{21–23} suggesting that the CDW's in thin blue-bronze samples are more coherent than in the large samples (volume of $\sim 10^{-4}$ cm³) usually examined.

The NBN frequency f_{NBN} varies linearly with the excess CDW current I_{CDW} . I_{CDW} is given by

$$I_{CDW} = I - \frac{V_{dc}}{R_0}, \quad (4)$$

where I is the total sample current, V_{dc} is the sample dc bias voltage, and R_0 is the sample low-field ($V_{dc} < V_T$) dc resistance. The linear relationship between I_{CDW} and f_{NBN} was found to hold true for the entire frequency range examined experimentally (≤ 150 kHz). Hence, strongly coherent $K_{0.3}MoO_3$ samples do not exhibit any deviation from a linear CDW-current-to-NBN-frequency relationship. The ratio between the NBN frequency and the CDW current density for the sample considered here was found to be $f_{NBN}/J_{CDW} = 12 \pm 3$ kHz cm²/A.

We have also examined the narrow-band-noise spectra of blue-bronze samples with volumes larger than that whose NBN spectrum is shown in Fig. 1. In general, the NBN quality drops sharply as the volume of the crystal examined varies from that of a transparent sample (volume of $\sim 10^{-8}$ cm³) to that of a more typical, bulk sample (volume of $\sim 10^{-4}$ cm³). In varying the volume from 10^{-8} to 10^{-4} cm³, the NBN peaks progressively become smaller in size and larger in width. In the large-volume limit, the noise spectrum displays no narrow-band peaks, but instead exhibits a fairly continuous noise distribution out to a critical frequency f_c .²⁴ Beyond f_c the noise level drops to zero. We find that this critical frequency varies linearly with the sample bias. These results clearly suggest that NBN generation in $K_{0.3}MoO_3$ is a bulk phenomenon, in agreement with research concerning NBN generation in NbSe₃.⁵

The effects of joint ac and dc driving fields on the differential resistance of the 0.2- μ m-thick $K_{0.3}MoO_3$ sample are shown in Fig. 2. The upper trace shows the

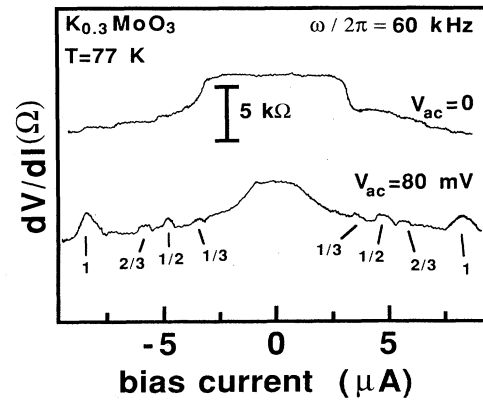


FIG. 2. Ac-dc interference effects in $K_{0.3}MoO_3$ at 77 K. The top trace is with no ac signal, while the bottom trace shows the differential resistance in the presence of a 60-kHz and 80-mV ac signal. The two traces have been vertically offset for clarity.

sample's current-driven differential resistance in the absence of any external ac signal. The CDW clearly depins at a threshold current of $I_T = 2.5$ μ A, beyond which dV/dI smoothly decreases as the CDW proceeds to slide. The bottom trace shows the changes in the differential resistance when it is measured with an additional 60-kHz ac signal of magnitude $V_{ac} = 80$ mV = $4V_T$ applied across the sample. This trace shows a number of partially-mode-locked Shapiro steps, each of which is labeled in the figure according to its index n . The fundamental harmonic ($n=1$) as well as three subharmonic ($n=1/3, 1/2,$ and $2/3$) steps are visible in Fig. 2. The lower trace also indicates that the mode-locking quality depends on the direction of the current bias, with the locking quality for negative biases being higher than for positive biases.

The degree to which the CDW becomes locked to the external ac signal is a strong function of the ac amplitude V_{ac} . This is shown in Fig. 3, where the Shapiro-step spectrum in a 40-kHz ac field is depicted as a function of V_{ac} . V_{ac} varies from 20 mV (V_T) to 120 mV ($6V_T$). The data in Fig. 3 indicate that the Shapiro-step height increases with increasing V_{ac} , up to roughly 80 mV, beyond which it begins to decrease again. This is more clearly shown in Fig. 4, where the Shapiro-step magnitude δV , the area under a Shapiro step in a (dV/dI) -versus- I trace, is plotted as a function of V_{ac} for the $n=1$ Shapiro step. This general step-height and step-magnitude dependence on V_{ac} appears to hold true for both harmonic and subharmonic Shapiro steps. Increasing V_{ac} also acts to decrease the CDW threshold current, and to move a given Shapiro step to progressively lower total current biases. Effects similar to these have also been observed in mode-locking experiments performed on NbSe₃ crystals.^{7,8,10}

To ensure that the mode-locking condition as stated in Eq. (3) holds for blue bronze, we have measured the CDW current density on each locked step as a function of the external locking frequency $\omega/2\pi$. The results for $n=2, 1,$ and $1/2$ are presented in Fig. 5. We find that the CDW current density on a particular mode-locked step

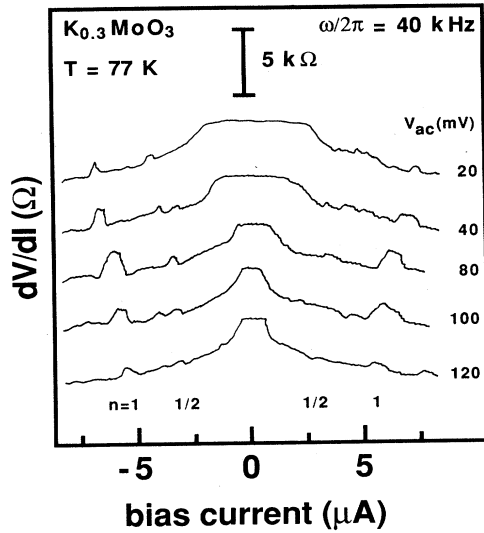


FIG. 3. Shapiro-step spectrum at 77 K with a 40-kHz ac signal. The ac amplitude varies from 20 mV (V_T) to 120 mV ($6V_T$). The traces are vertically offset for clarity.

J_{lock} is independent of the ac amplitude for the entire range of measurements ($V_{\text{ac}} \leq 6V_T$). The NBN frequency as a function of CDW current density is also plotted in the figure. These data indicate that J_{lock} is linearly related to the locking frequency for all three values of n . The empirical locking-CDW-current-density-to-locking-frequency ratio is $f_{\text{ex}}/J_{\text{lock}} = \beta/n$, where $\beta = 12 \pm 3$ kHz cm^2/A .

We now turn to an examination of dc-bias effects on the complex ac conductivity $\sigma(\omega)$ in $\text{K}_{0.3}\text{MoO}_3$. In these experiments, a small-amplitude ($V_{\text{ac}} \ll V_T$) ac signal $V = V_{\text{ac}} \cos(\omega t)$ is applied across the sample and the resulting current I_{ac} flowing through the sample at the same frequency is detected. A bias voltage V_{dc} may also

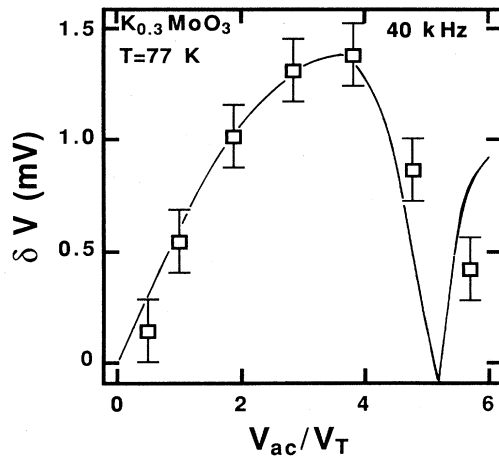


FIG. 4. Shapiro-step magnitude δV plotted as a function of the applied ac driving signal amplitude. The external ac frequency was set at $\omega/2\pi = 40$ kHz. The solid line is a fit to the data (see text).

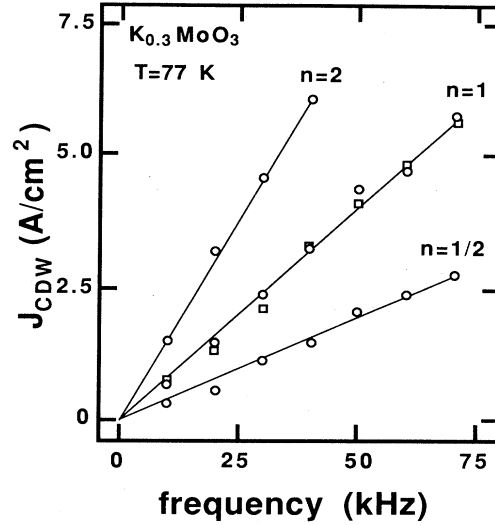


FIG. 5. CDW current density plotted as a function of external locking frequency for both Shapiro-step data (circles) and narrow-band-noise data (squares).

be applied. The complex conductivity, $\sigma(\omega) = \text{Re}\sigma(\omega) + i \text{Im}\sigma(\omega)$, is determined from

$$\sigma(\omega) = \frac{L}{A} \frac{I_{\text{ac}}}{V_{\text{ac}}} e^{i\theta}, \quad (5)$$

where A is the sample cross-sectional area, L is its length, and θ reflects the component of the current response which is out of phase with the input voltage. Our zero-bias complex-conductivity measurements on thin samples of $\text{K}_{0.3}\text{MoO}_3$ at 77 K show a rise in $\text{Re}\sigma(\omega)$ beginning at roughly 20 kHz; this low-frequency mode is the extensively studied dielectric relaxation mode apparently present in all completely gapped depinnable CDW materials.^{14,15} The rise in $\text{Re}\sigma(\omega)$ indicates that the characteristic frequency f_{DR} for this mode is roughly 20 kHz.

The effects on the 50-kHz complex conductivity when a depinning bias field is applied to a thin $\text{K}_{0.3}\text{MoO}_3$ sample are depicted in Fig. 6. The real part of the conductivity is presented in Fig. 6(a), while the dielectric constant ϵ , given by

$$\epsilon(\omega) = \frac{4\pi \text{Im}\sigma(\omega)}{\omega}, \quad (6)$$

is presented in Fig. 6(b). There is very little change in $\text{Re}\sigma(\omega)$ for $I_{\text{dc}} < I_T = 2.5 \mu\text{A}$, while $\epsilon(\omega)$ does show a slight increase just below threshold. Past threshold, the complex conductivity changes drastically: the real part of the conductivity begins to increase while the dielectric constant decreases towards zero. In addition to this general depinning response, both $\text{Re}\sigma(\omega)$ and $\epsilon(\omega)$ exhibit distinct anomalies for well-defined values of the bias current. In particular, $\epsilon(\omega)$ displays a well-defined inductive ($\Delta\epsilon < 0$) dip at $I_{\text{dc}} = 5.7 \mu\text{A}$, and a smaller dip at $I_{\text{dc}} = 4.3 \mu\text{A}$. Anomalies at these bias currents also show up in $\text{Re}\sigma(\omega)$. The feature in $\text{Re}\sigma(\omega)$ centered around $I_{\text{dc}} = 5.7 \mu\text{A}$ is particularly noticeable. This anomaly is characterized by a *drop* below the background CDW con-

ductivity at a value of I_{dc} just below that which gives the large inductive dip in $\epsilon(\omega)$. A similar rise above the background conductivity occurs for values of I_{dc} slightly larger than the inductive dip bias. An examination of the NBN spectrum shows that, for $I_{dc}=5.7 \mu\text{A}$, $f_{\text{NBN}}=50 \text{ kHz}$, while at $I_{dc}=4.3 \mu\text{A}$ the second NBN harmonic occurs at 50 kHz. This suggests that the anomalies at 4.3 and 5.7 μA are related to resonances between the 50-kHz probing signal and the second NBN harmonic or the NBN fundamental, respectively. Similar well-defined anomalies have been extensively studied in NbSe_3 .^{7,10} Very broad anomalies at low frequencies have also been previously reported for $\text{K}_{0.3}\text{MoO}_3$.¹²

The bias current at which the strong resonance anomalies occur should be a strong function of the probe frequency since they occur when the internal NBN frequency matches the probing frequency. This is shown to be the case in Fig. 7, where the dielectric constant $\epsilon(\omega)$ is plotted as a function of bias current for several ac probing frequencies. The resonance current bias clearly scales linearly with the ac frequency. This is evident in Fig. 8, where the CDW current density at resonance is plotted as a function of the resonance frequency. The experimental

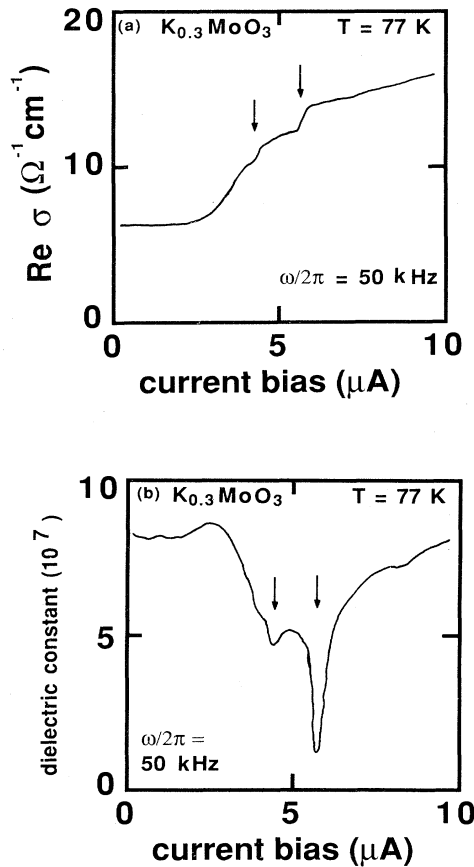


FIG. 6. (a) The real part of the ac conductivity, $\text{Re}\sigma(\omega)$, measured at $\omega/2\pi=50 \text{ kHz}$ as a function of dc-bias current. (b) The dielectric constant $\epsilon(\omega)$ measured at $\omega/2\pi=50 \text{ kHz}$ as a function of dc-bias current.

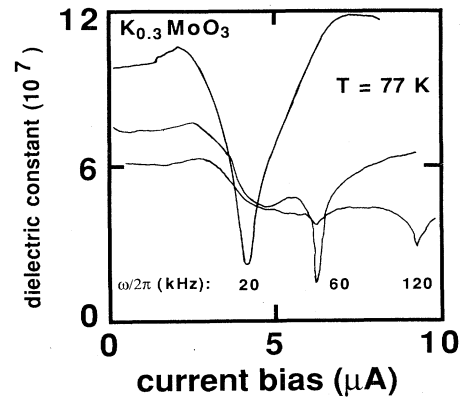


FIG. 7. The dielectric constant $\epsilon(\omega)$ measured as a function of dc-bias current at three frequencies (20, 60, and 120 kHz).

NBN frequency f_{NBN} to CDW current density relationship is also plotted in the figure. Clearly, both sets of data lie on a line which has a slope of $f_{\text{NBN}}/J_{\text{CDW}}=12 \text{ kHz cm}^2/\text{A}$. This conclusively shows that the anomalies which appear in both $\epsilon(\omega, I_{dc})$ and $\text{Re}\sigma(\omega, I_{dc})$ are caused by a direct interference between the internal NBN signal at f_{NBN} and the external signal at $\omega/2\pi$.

Returning to the data in Fig. 7, the placement of the inductive dip is not the only frequency-dependent aspect of $\epsilon(\omega, I_{dc})$. The below-threshold dielectric constant appears to decrease with increasing frequency. Additionally, the depth of the inductive dip also decreases with increasing frequency. At 20 kHz, the change in $\epsilon(\omega)$ due to the dip is $\Delta\epsilon(20 \text{ kHz})=-8 \times 10^7$, while at 120 kHz it is only $\Delta\epsilon(120 \text{ kHz})=-1.4 \times 10^7$. At frequencies below 20 kHz, the dip continues to increase in size. This is shown in Fig. 9, where the bias-dependent dielectric constant is plotted at 1, 40, 80, and 120 kHz. The inductive dip measured at 1 kHz clearly dwarfs the anomalies at the higher frequencies; the size of the dip at 1 kHz is

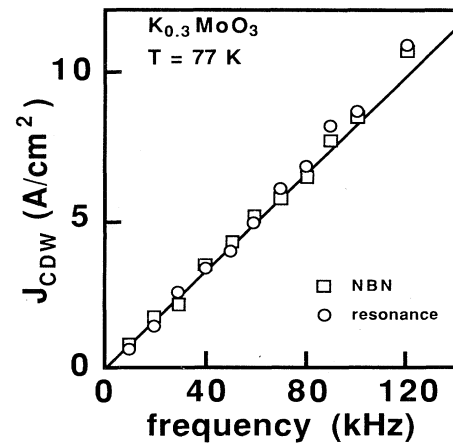


FIG. 8. The CDW current density at resonance plotted as a function of the resonance frequency (circles). The CDW-current-density-to-NBN-frequency (f_{NBN}) ratio is also plotted in the figure (squares).

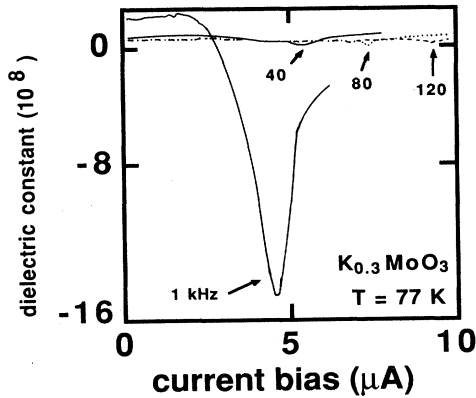


FIG. 9. $\epsilon(\omega, I_{dc})$ at low (1 kHz) and high frequencies (40, 80, and 120 kHz). The comparatively small high-frequency resonances are indicated by arrows.

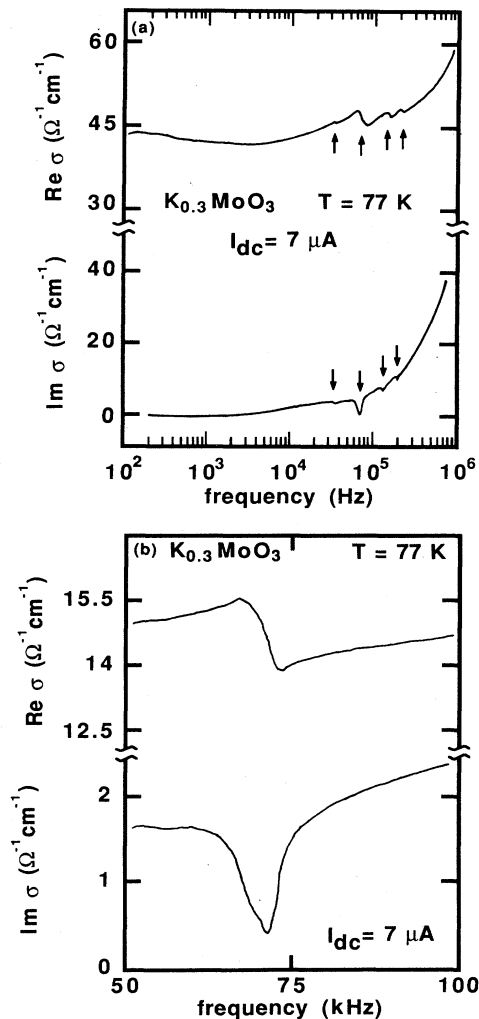


FIG. 10. (a) Real and imaginary parts of the conductivity in the presence of a depinning current bias of $I_{dc} = 7 \mu\text{A}$. At this bias, the NBN fundamental occurs at $f_{\text{NBN}} = 70 \text{ kHz}$. The harmonic resonances at 35, 70, 140, and 210 kHz are indicated by arrows. In (b) a close up around the 70-kHz resonance is shown in a linear-frequency-scale representation.

$\Delta\epsilon(1 \text{ kHz}) = -160 \times 10^7$, a factor of 114 higher than the dip at 120 kHz. This indicates that $\Delta\epsilon$ diverges as $1/\omega$ in the limit that ω goes to zero.

The anomalies in the complex ac conductivity depicted in Figs. 6, 7, and 9 are observed by measuring $\sigma(\omega)$ at a fixed frequency while varying the dc bias. Presumably, the same effects should occur when the dc bias is held fixed and the measurement frequency is swept. The frequency-dependent ac conductivity at a depinning bias of $I_{dc} = 7 \mu\text{A}$ is depicted in Fig. 10. At this bias, the NBN fundamental occurs at $f_{\text{NBN}} = 70 \text{ kHz}$. Inductive dips are clearly present in the imaginary part of the conductivity at $\omega/2\pi = f_{\text{NBN}}/2$ (35 kHz), f_{NBN} (70 kHz), $2f_{\text{NBN}}$ (140 kHz), and $3f_{\text{NBN}}$ (210 kHz). In addition, anomalies show up in $\text{Re}\sigma(\omega)$ centered about these four frequencies. The anomaly at 70 kHz is larger than those at the other frequencies. Details of the resonance around this frequency are shown in Fig. 10(b), where the ac conductivity is plotted versus frequency utilizing a linear frequency scale. The imaginary part of the conductivity exhibits an inductive dip with a magnitude of $1.3 (\Omega \text{ cm})^{-1}$. $\text{Re}\sigma(\omega)$ shows a smaller, less pronounced positive and negative set of peaks above and below 70 kHz, respectively. These two peaks have equal magnitudes of $0.7 (\Omega \text{ cm})^{-1}$ above and below the background CDW-plus-normal-electron conductivity of roughly $15 (\Omega \text{ cm})^{-1}$. At the 70-kHz resonance frequency, $\text{Re}\sigma(\omega)$ appears unchanged from the background-conductivity value.

IV. ANALYSIS

We first examine the relationship between the CDW current density and the NBN frequency in blue bronze. The three sets of experiments discussed in the preceding section provide an accurate estimate of the ratio $f_{\text{NBN}}/J_{\text{CDW}}$, which can be directly compared to an expression which holds true for NBN phenomena in both NbSe_3 and TaS_3 . We next use a simple single-particle classical model of CDW dynamics to analyze the Shapiro-step-magnitude dependence on ac signal amplitude. Lastly, we will discuss the underlying mechanisms which cause the resonance features in the dc-biased complex ac conductivity.

A. CDW-current-density-to-NBN-frequency relationship

A simple model³ predicts that the fundamental NBN frequency is linearly related to the CDW current density by

$$\frac{f_{\text{NBN}}}{J_{\text{CDW}}} = \frac{1}{n_c e \lambda_{\text{pin}}}, \quad (7)$$

where λ_{pin} is the intrinsic pinning potential wavelength, and n_c is the CDW electronic carrier concentration. NBN studies indicate that Eq. (7) holds true for both NbSe_3 and TaS_3 .^{3,25} It has been suggested that for CDW conductors the pinning-potential wavelength is equal to the CDW wavelength ($\lambda_{\text{pin}} = \lambda_{\text{CDW}}$). There has been some controversy as to whether or not Eq. (7) holds true for $\text{K}_{0.3}\text{MoO}_3$.^{12,21-23} A large variation exists in the

values reported for $f_{\text{NBN}}/J_{\text{CDW}}$ based on NBN measurements. This is due primarily to the low-quality NBN spectra typically exhibited by $\text{K}_{0.3}\text{MoO}_3$ samples. The very-high-quality spectra displayed by our thin samples make a determination of λ_{pin} from Eq. (7) more reliable. With the measured ratio $f_{\text{NBN}}/J_{\text{CDW}} = 12 \pm 3$ $\text{kHz cm}^2/\text{A}$, the measured sample dimensions, and using $n_c = 4.98 \times 10^{21} \text{ cm}^{-3}$ as determined from structural considerations (see below),¹³ Eq. (7) yields a pinning-potential periodicity $\lambda_{\text{pin}} = 10.5 \pm 2 \text{ \AA}$. This length is in close agreement with the CDW wavelength in $\text{K}_{0.3}\text{MoO}_3$, $\lambda_{\text{CDW}} = 9.9 \text{ \AA}$. Thus, in this material, $\lambda_{\text{pin}} = \lambda_{\text{CDW}}$. Our observed $f_{\text{NBN}}/J_{\text{CDW}}$ ratio, and hence the determined value of λ_{pin} , is in agreement with recent NMR measurements.^{26,27}

The method employed here to determine λ_{pin} clearly requires an accurate estimate of the CDW carrier concentration n_c . The value used here is arrived at by a simple potassium-counting argument.¹³ The $\text{K}_{0.3}\text{MoO}_3$ unit cell contains 20 formula units, and the potassium ions provide the free carriers in the material. With six K ions per unit cell (volume of 1205 \AA^3), each providing one electron, a carrier concentration of $n_e = 4.98 \times 10^{21} \text{ cm}^{-3}$ results. The 180-K Peierls transition completely gaps the Fermi surface in blue bronze, and hence $n_c = n_e$. Band-structure calculations indicate that the complete unit cell produces four degenerate conduction bands (two bands per $\text{Mo}_{10}\text{O}_{30}$ cluster) at the Fermi surface.^{13,28,29} The measured Fermi wave vector of $\frac{3}{4}b^*$ is thus consistent with there being six electrons per unit cell. Additionally, n_e as determined from Hall-effect data³⁰ agrees with the carrier concentration as estimated by the above-mentioned counting argument. Hence, both band-structure considerations and Hall-effect data support the notion that $n_c = 4.98 \times 10^{21} \text{ cm}^{-3}$ in $\text{K}_{0.3}\text{MoO}_3$ as estimated from the simple electron-counting scheme.

The value of λ_{pin} may also be determined from the Shapiro-step interference data. During mode locking the locking frequency f_{ex} and CDW current density J_{lock} are related by

$$\frac{f_{\text{ex}}}{J_{\text{lock}}} = \frac{1}{n} \frac{f_{\text{NBN}}}{J_{\text{CDW}}}, \quad (8)$$

where n is the Shapiro-step index. The data in Fig. 5 give a value for this ratio of $f_{\text{ex}}/J_{\text{lock}} = \beta/n$, with $\beta = 12 \pm 3$ $\text{kHz cm}^2/\text{A}$. Therefore, the Shapiro-step data produce a value for the NBN-frequency-to-CDW-current-density ratio of $f_{\text{NBN}}/J_{\text{CDW}} = 12 \pm 3$ $\text{kHz cm}^2/\text{A}$, in agreement with the ratio determined directly from NBN measurements.

The close correspondence between the value of $f_{\text{NBN}}/J_{\text{CDW}}$ as determined from the mode-locking experiments and from the narrow-band-noise spectrum reflects the very high quality of the noise spectrum. In other CDW materials, such as TaS_3 , inhomogeneous current densities within the sample often lead to a smeared noise spectrum and a nonlinear f_{NBN} -versus- J_{CDW} relationship;¹¹ in such cases, the application of a large-amplitude ac field may serve to homogenize the sample and linearize

the $f_{\text{NBN}}-J_{\text{CDW}}$ relationship. In our specimens of $\text{K}_{0.3}\text{MoO}_3$, a well-defined $f_{\text{NBN}}/J_{\text{CDW}}$ ratio can be obtained even in the absence of large ac drive amplitude.³¹

B. Mode locking

In this subsection we will examine the quantitative nature of mode locking in blue bronze, particularly the dependence of the Shapiro-step magnitude δV on the amplitude of the applied ac locking signal. The data are analyzed within a simple model which qualitatively accounts for Shapiro steps observed in NbSe_3 .^{7,8}

A number of models have been proposed to account for CDW dynamics. Both single-degree-of-freedom⁸ and many-internal-degrees-of-freedom^{32,33} models have been proposed to account for ac-dc interference effects. A simple single-degree-of-freedom phenomenological model,¹⁸ which treats the CDW as an object with charge e and mass m^* moving in a sinusoidal potential, has been surprisingly successful in qualitatively and semiquantitatively describing the essential frequency- and electric-field-dependent features of CDW transport.² The single-particle equation of motion is¹⁸

$$\frac{d^2x}{dt^2} + \Gamma \frac{dx}{dt} + \frac{\omega_0^2}{Q} \sin(Qx) = \frac{eE}{m^*}, \quad (9)$$

where x is the CDW center-of-mass coordinate, E is the applied electric field, Q is the periodic pinning-potential wave vector, ω_0 is the characteristic resonance frequency of the CDW, and $\Gamma = 1/\tau$ is a damping constant with a characteristic relaxation time τ ; Eq. (7) follows directly from Eq. (9) with $Q = 2\pi/\lambda_{\text{pin}}$. This model accounts for both the narrow-band-noise oscillations and mode locking observed in CDW materials. In addition, it quantitatively describes the Shapiro-step-magnitude dependence on ac signal amplitude in NbSe_3 .^{7,8} From our determination that $\lambda_{\text{pin}} = \lambda_{\text{CDW}}$ in $\text{K}_{0.3}\text{MoO}_3$, we set $Q = 2\pi/\lambda_{\text{CDW}}$ in Eq. (9).

In analogy with the Stewart-McCumber model of Josephson tunneling,³⁴ Eq. (9) predicts that the magnitude of the $n = 1$ Shapiro step in the high-frequency limit ($\omega_{\text{ex}} \gg \omega_0^2\tau$) should be⁸

$$\delta V = 2\alpha V_T(\omega=0) \left| J_1 \left[\frac{\omega_0^2\tau}{\omega} \frac{V_{\text{ac}}}{V_T(\omega=0)} \right] \right|, \quad (10)$$

where α represents the volume fraction locked to the external signal, while ω and V_{ac} are the frequency and amplitude of the applied signal, respectively. In the low-frequency (overdamped) limit ($\omega \leq \omega_0^2\tau$) the inertial term (d^2x/dt^2) can be neglected, and a modified Bessel-like solution for δV can be obtained numerically.³⁵ In the extreme low-frequency limit ($\omega \ll \omega_0^2\tau$), the numerical solution predicts that δV has a maximum at $V_{\text{ac}} = V_T$ with an amplitude of $\delta V = (\omega/\omega_0^2\tau)V_T$.

Recently, a seemingly more general derivation for the Shapiro-step magnitude was published.¹⁰ That derivation utilized a model-independent approach and assumed that the pinning potential was in the form of a cusped-cosine function. Although one might assume that this approach

should yield a more general, model-independent result, it can be shown³⁶ that the resulting expression for δV is exactly equivalent to that produced by a single-particle model with a cusped-cosine, rather than a sinusoidal, potential. Nonetheless, this approach clears up two deficiencies of Eq. (10). First, the new result correctly predicts the existence of subharmonic Shapiro steps. Second, because the expression for δV involves a summation of Bessel functions weighted by the pinning potential's Fourier coefficients, the Shapiro-step magnitude does not go to zero at the minima [in contrast to the predictions of Eq. (10)]. Both of these qualitative enhancements are directly related to the inclusion of higher harmonics in the pinning potential. Unfortunately, the model's quantitative prediction [locations of maxima and minima in $\delta V(V_{ac})$] have yet to be compared to experimental data due to the complexity of the expression. Therefore, it is unclear if the approach of Ref. 10 is quantitatively superior to Eq. (10). For this reason, we shall analyze the blue-bronze mode-locking data by using the predictions of the single-particle classical model, Eq. (9).

A reasonable fit to the data in Fig. 4 can be obtained by utilizing the numerical low-frequency solution presented in Ref. 34 and considering $\omega_0^2\tau$ to be a fitting parameter. The solid-line fit in Fig. 4 was obtained in this way with $f_0 = \omega_0^2\tau/2\pi = 25$ kHz. It is noteworthy that this value is roughly 6 orders of magnitude below the characteristic frequency of the high-frequency pinned mode seen in $K_{0.3}MoO_3$ (~ 10 GHz).¹⁷ According to Eq. (9), the contribution to δV from the 10-GHz pinned mode would be negligible at the frequencies where these measurements were performed (40 kHz). Further, low-frequency ac-conductivity measurements indicate that the dielectric relaxation mode in the sample considered here has a characteristic frequency of $f_{DR} \approx 20$ kHz. Hence, it appears that the ac-dc interference effects seen in $K_{0.3}MoO_3$ at 77 K are a result of interactions between the external ac signal and the low-frequency dielectric relaxation mode present in this material.

By considering in greater detail the low-frequency behavior of blue bronze, it becomes clear that the observed ac-dc interference effects must relate to the low-frequency mode. In particular, the narrow-band-noise frequencies typically produced by $K_{0.3}MoO_3$ crystals are relatively low, between 10 and 100 kHz. In addition, dc CDW motion has been shown to be strongly damped below 100 K, with the degree of damping growing with decreasing temperature.³⁷ The damping is such that the CDW conductivity in dc electric fields, far in excess of the threshold field, is limited to the normal carrier Ohmic conductivity. The NBN frequency and dc conductivity predicted by Eq. (9) are

$$f_{NBN}(E) = \frac{1}{2\pi} \frac{Q\tau e}{m^*} E g(E) \quad (11)$$

and

$$\sigma_{dc}(E) = \frac{n_c e^2 \tau}{m^*} g(E), \quad (12)$$

respectively, where $g(E)$ is a function of the applied electric field E with the limiting behavior: $g(E \leq E_T) = 0$ and $g(E \gg E_T) = 1$. Equations (11) and (12) indicate that large CDW damping (small τ) is responsible for low dc CDW conductivities and NBN frequencies (small NBN frequencies and CDW conductivities cannot be attributed to variations in Q or m^* because both are tied to the CDW gap). This suggests that the small characteristic frequency $\omega_0^2\tau$ in blue bronze stems from large CDW damping.

An estimate of $\omega_0^2\tau$ can be obtained from the experimental data by considering the threshold dc electric field in the single-particle model. From Eq. (9) the threshold field E_T is

$$E_T = \frac{m^*}{Qe} \omega_0^2. \quad (13)$$

This yields an expression for $\omega_0^2\tau$ in terms of E_T and $Qe\tau/m^*$. To obtain $\omega_0^2\tau$ in terms of experimentally determinable quantities, we utilize the high-field limit of Eq. (12) [$g(E) = 1$], as well as the NBN-frequency-to-CDW-current-density relation [Eq. (7)]. By substituting these expressions into Eq. (13), $f_0 = \omega_0^2\tau/2\pi$ becomes

$$f_0 = \frac{f_{NBN}}{J_{CDW}} \sigma_{dc}(E \gg E_T) E_T. \quad (14)$$

The pertinent experimentally determined parameters for the sample considered here are $f_{NBN}/J_{CDW} = 12 \pm 3$ kHz cm²/A, $E_T = 320$ mV/cm, and $\sigma_{dc}(E \gg E_T) = 10$ (Ω cm)⁻¹. Based on these numbers, Eq. (14) yields a value of $f_0 = 38 \pm 10$ kHz. This result is in reasonable order-of-magnitude agreement with the frequencies determined from both the fit to the Shapiro-step data ($f_0 = 25$ kHz) and from the ac-conductivity measurements ($f_{DR} \approx 20$ kHz). Hence, it appears that Eq. (9) roughly accounts for the fundamental frequency of the low-temperature dielectric relaxation mode in blue bronze. Further, the analysis indicates that the low-frequency ac-dc interference effects in this material are a direct result of the external signals interacting with the low-frequency dielectric relaxation mode.

This analysis suggests that large CDW damping is responsible for relatively low CDW conductivities, NBN frequencies, and characteristic dielectric-relaxation-mode frequencies associated with the sliding CDW state in $K_{0.3}MoO_3$. Tucker *et al.*³⁸ recently pointed out that the Arrhenius behavior displayed by the characteristic frequency of the dielectric relaxation mode closely matches the activated temperature-dependent behavior exhibited by the low-field resistance R_0 in $K_{0.3}MoO_3$. Based on the close correspondence between $f_{DR}(T)$ and $R_0(T)$, Tucker *et al.* suggest that both the strong CDW damping and the low-frequency dielectric relaxation mode that occur in $K_{0.3}MoO_3$ result from normal carrier screening of charge polarizations present in the CDW when in electric fields below threshold.

The low-frequency interference effects evident in blue bronze are analogous to those seen in $NbSe_3$ at higher frequencies.^{7,8,10} Hence, both the low-frequency and high-

frequency conductivity modes in CDW materials appear to be qualitatively similar. This lends support to the theories concerning screening effects of normal electrons on the CDW as first discussed by Sneddon³³ and more recently by both Tucker *et al.*³⁸ and Littlewood.³⁹ In completely gapped CDW materials, normal electrons act to screen the moving CDW, leading to an enhancement in CDW damping and the creation of an overdamped, low-frequency pinned mode. This screening action can only take place in the low-frequency (≤ 10 MHz) limit. In the high-frequency (> 100 MHz) limit, normal electrons are ineffective in damping CDW motion, and an additional unscreened and underdamped, "bare" high-frequency pinned-phonon mode should be realized. The Shapiro-step data presented here provide direct evidence that these two modes are qualitatively similar in that external driving fields can couple to them in an analogous manner.

C. ac-conductivity resonances

The data presented in Figs. 6–10 clearly indicate that a resonancelike anomaly occurs in $\sigma(\omega)$ when the internal NBN frequency or one of its harmonics coincides with the frequency at which the ac conductivity is being measured. In this section we examine the detailed nature of these resonant anomalies.

The anomalies appear as sharp inductive dips in either $\text{Im}\sigma(\omega)$ or $\epsilon(\omega)$. The corresponding feature in $\text{Re}\sigma(\omega)$ appears as gradual positive and negative peaks located equidistant above and below the resonance position, respectively. At resonance, $\text{Re}\sigma(\omega)$ appears unchanged from its inferred value if no resonance had occurred. A comparison of the anomalies in $\text{Re}\sigma(\omega)$ for bias-swept data [Fig. 6(a)] and for frequency-swept data [Fig. 10(b)] shows that the ordering of the positive and negative peaks relative to the central resonance position are interchanged in the two cases. For bias sweeps, a negative peak occurs just below resonance ($f_{\text{NBN}} < \omega/2\pi$), while for frequency sweeps this negative peak occurs above the resonance ($\omega/2\pi > f_{\text{NBN}}$). This suggests that the parameter which best characterizes the resonance condition is

$$\Delta f = f_{\text{NBN}} - \frac{\omega}{2\pi}. \quad (15)$$

Regardless of which parameter is swept, $\text{Re}\sigma(\omega)$ shows a rounded positive peak when Δf approaches zero from above ($\Delta f > 0$) and a negative peak when approaching zero from below ($\Delta f < 0$). In either case, a sharp negative peak occurs in $\text{Im}\sigma(\omega)$ centered at $\Delta f = 0$.

The response at resonance is functionally analogous to a resonant harmonic oscillator, but with a phase shift which allows the main resonance at $\Delta f = 0$ to occur as a negative peak in $\text{Im}\sigma(\omega)$. To better understand this phenomenon, we consider the response of the sample to a low-amplitude ($V_{\text{ac}} \ll V_T$) ac signal in combination with a depinning dc bias $V = V_{\text{dc}} + V_{\text{ac}}\cos(\omega t)$.⁷ The normal carriers will respond with a current $I_n \cos(\omega t)$ completely in phase with the ac signal. The CDW responds with a current $I_{\text{CDW,ac}}\cos(\omega t + \theta)$, where the phase angle θ reflects the fact that the CDW conductivity has both a real and an imaginary component ($\theta \neq 0$). In addition to these signals, there is the CDW current produced by the

dc bias. This includes both a dc current $I_{\text{CDW,dc}}$ and an oscillating current related directly to the narrow-band noise, $I_{\text{NBN}}h(\omega_{\text{NBN}}t + \phi)$, where h is a periodic function with a period $1/\omega_{\text{NBN}}$. The function $h(\omega t)$ can be well approximated by a complex sinusoidal function $e^{i\omega t}$. The complete current response becomes

$$I = I_{\text{CDW,dc}} + e^{i\omega t}(I_n + I_{\text{CDW,ac}}e^{i\theta} + I_{\text{NBN}}e^{i\phi}). \quad (16)$$

The total ac conductivity at the probe frequency ω is

$$\sigma(\omega) = \left\langle \frac{I}{V} \right\rangle = \frac{I_n}{V_{\text{ac}}} + \frac{I_{\text{CDW,ac}}}{V_{\text{ac}}} e^{i\theta} + \frac{I_{\text{NBN}}}{V_{\text{ac}}} \delta_{\omega\omega_{\text{NBN}}} e^{i\phi}, \quad (17)$$

where the angular brackets ($\langle \rangle$) denote a time average, and δ_{ab} is a Kronecker delta. For $\omega \neq \omega_{\text{NBN}}$, only the normal and CDW conductivities contribute to the measurement. For $\omega = \omega_{\text{NBN}}$, an extra contribution to the conductivity will result from the NBN signal. In order for the resonant conductivity enhancement to appear as a negative dip in the out of phase component, the phase angle at resonance must be $\phi = -\pi/2$.

The size of the inductive dip is predicted by Eq. (17) to be

$$\Delta \text{Im}\sigma(\omega = \omega_{\text{NBN}}) = \frac{L}{A} \frac{I_{\text{NBN}}}{V_{\text{ac}}}. \quad (18)$$

This expression makes a number of specific predictions about the inductive dip which can be directly compared to the data presented in Figs. 6–10. First, Eq. (18) suggests that because the size of the NBN oscillations depend only on the dc bias and not on the ac magnitude or frequency, the magnitude of the inductive dip should be independent of the frequency at which the resonance occurs. The measured dip magnitude $\Delta \text{Im}\sigma$ is plotted as a function of the resonance frequency in Fig. 11. Clearly, $\Delta \text{Im}\sigma$ is independent of the resonance frequency, with a value of $\Delta \text{Im}\sigma = 1.0 \pm 0.1 (\Omega \text{ cm})^{-1}$. This can be directly compared to experimental parameters; with an ac signal

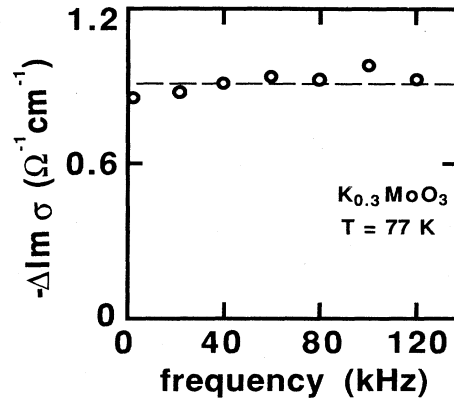


FIG. 11. The magnitude $\Delta \text{Im}\sigma(\omega)$ of the inductive dip in the imaginary part of the conductivity at resonance. The dip magnitude is roughly independent of frequency, with an average value of $1.0 \pm 0.1 (\Omega \text{ cm})^{-1}$ as indicated by the dashed line in the figure.

amplitude of $V_{ac}=1$ mV and a NBN current of $I_{NBN}=10\pm 3$ nA ($100\ \mu\text{V}$ across $10\ \text{k}\Omega$), Eq. (18) predicts a dip magnitude of $\Delta\text{Im}\sigma=0.6\pm 0.2$ ($\Omega\ \text{cm}$)⁻¹, in reasonable agreement with the measured value. With $\Delta\text{Im}\sigma$ independent of frequency, the ac dielectric constant should be inversely proportional to ω , in agreement with the data presented in Figs. 7 and 9. The inclusion of I_{NBN} in Eq. (18) also indicates why the resonances involving NBN harmonics are smaller than the resonance involving the fundamental NBN peak. This arises from the fact that magnitude I_{NBN} of a harmonic NBN peak drops as the harmonic order increases. Lastly, Eq. (18) would suggest that, for $V_{ac}\ll V_T$, increasing V_{ac} should, in turn, decrease the relative size of the resonance anomaly. Although $\Delta\text{Im}\sigma$ was not measured as a function of V_{ac} here, a reduction of $\Delta\text{Im}\sigma$ with increasing V_{ac} has been observed in NbSe₃.¹⁰

We now consider the resonance anomaly in $\text{Re}\sigma(\omega)$. By a simple Kramers-Kronig analysis, positive and negative peaks in $\text{Re}\sigma(\omega)$ must occur if a sharp, negative resonant peak appears in $\text{Im}\sigma(\omega)$. In terms of the harmonic-oscillator analogy discussed earlier, it would appear that off (but near) resonance ($\Delta f\neq 0$) the phase ϕ of the NBN signal relative to the ac probing signal must depart from the value at resonance ($\phi=-\pi/2$). In order to correctly account for the signs of the peaks in $\text{Re}\sigma(\omega)$ above and below $\Delta f=0$, this phase angle must have the limiting behavior $\phi=-\pi$ for $\Delta f\ll 0$, and $\phi=0$ for $\Delta f\gg 0$. Further, the harmonic-oscillator analogy would suggest that the inductive dip $\Delta\text{Im}\sigma$ should be twice as large as the size $\Delta\text{Re}\sigma$ of the peaks in $\text{Re}\sigma$. The ratio of these magnitudes in Fig. 6 is $(\Delta\text{Im}\sigma)/(\Delta\text{Re}\sigma)=1.7$, while in Fig. 10 it is $(\Delta\text{Im}\sigma)/(\Delta\text{Re}\sigma)=1.9$. Both values are in reasonable accord with the factor-of-2 harmonic-oscillator prediction.

The ac-conductivity resonance effects reported here differ from those previously observed in NbSe₃ only in the relative sharpness of the anomalies in $\text{Re}\sigma$. In NbSe₃, the anomaly appears more as a steplike feature than as a pair of positive and negative peaks. The relative sharpness of this feature in a resonant harmonic oscillator is controlled by the damping parameter. With large damping, the resonance is broad and a pair of gradual peaks appear in the out-of-phase conductivity centered about the resonance frequency. As the damping falls to zero, these two features form into a sharp steplike anomaly which occurs exactly at resonance. This suggests that the damping related to the resonance in K_{0.3}MoO₃ is larger than that in NbSe₃. As discussed in the preceding section, the CDW in blue bronze is highly damped below $100\ \text{K}$,^{33,39} whereas the CDW's in NbSe₃ are not effectively damped.³⁹ Hence, it would appear that the differences between the resonant anomalies in these two materials directly reflect the different relative CDW damping that exists within them.

There is still no complete understanding of why the NBN oscillations are $-\pi/2$ out of phase with the probing signal at resonance. The general features of these resonances in $\sigma(\omega)$ have been accounted for by numerical

solutions of both a Frenkel-Kontorova model³³ and the tunneling model¹⁰ [as yet, the predictions of the single-particle classical model, Eq. (9), have not been numerically calculated]. In both cases, no effort was made to understand why the NBN signal is $-\pi/2$ out of phase with respect to the probing signal at resonance. In voltage-driven pulsed mode-locking experiments, it has been found that the phases of the NBN oscillations are always $-\pi/2$ out of phase with respect to the start of the pulse.⁴⁰ Therefore, whatever the cause, the $-\pi/2$ phase shift between the NBN signal and an external ac signal at resonance appears to be a general feature of CDW response.

V. CONCLUSIONS

The results presented in this paper indicate that a highly coherent response can be obtained in very thin K_{0.3}MoO₃ samples. Further, this strongly coherent sliding CDW state can couple with combined ac and dc fields to cause a variety of interference effects which are analogous to those seen in NbSe₃ and TaS₃. In particular, the CDW can be mode locked to a large-amplitude ac driving signal, resulting in the formation of Shapiro steps in a sample's differential resistance. The relative height of the Shapiro steps observed in blue bronze indicate that upwards of 50% of the CDW becomes locked to the external ac field. In the presence of small-amplitude ac probing fields, the dc-biased complex ac conductivity shows strong resonance features due to the interactions between the NBN signal and the probing signal. Although a CDW is a many-particle system and, in general, must be described by a many-particle Hamiltonian, both of these phenomena can be accounted for by using a simple phenomenological single-particle equation of motion. This indicates that the CDW internal degrees of freedom can be neglected when describing, in a simple way, these ac-dc interference effects.

Analysis of the interference features present in the response of the CDW in K_{0.3}MoO₃ show evidence for strong damping of the charge-density wave. This is evident both in the low-frequency Shapiro-step data and in the relatively broad resonance features which appear in the real part of the conductivity when $\sigma(\omega)$ is measured in the presence of a depinning bias. Hence, although ac-dc interference phenomena appear to be universally exhibited by depinnable CDW's, underlying interactions within the CDW (i.e., internal degrees of freedom) manifest themselves as subtle variations in the overall resonant and mode-locked response.

ACKNOWLEDGMENTS

We thank M. F. Crommie, P. Parilla, and M. S. Sherwin for useful discussions. We also thank K. Zettl for growing the crystals used in this study. This research was supported by the U. S. National Science Foundation (NSF) under Grant No. DMR-84-00041. One of us (A.Z.) acknowledges support from the Alfred P. Sloan Foundation.

- *Present address: Los Alamos National Laboratory, Los Alamos, NM 87545.
- ¹P. Monceau, N. P. Ong, A. M. Portis, A. Meerschaut, and J. Rouxel, *Phys. Rev. Lett.* **37**, 602 (1976).
 - ²For a review, see G. Grüner and A. Zettl, *Phys. Rep.* **119**, 117 (1985); see also P. Monceau, in *Electronic Properties of Quasi-One-Dimensional Materials*, edited by P. Monceau (Reidel, Dordrecht, 1985), Vol. II, p. 139.
 - ³P. Monceau, J. Richard, and M. Renard, *Phys. Rev. Lett.* **45**, 43 (1980).
 - ⁴N. P. Ong, G. Verma, and K. Maki, *Phys. Rev. Lett.* **52**, 663 (1984); N. P. Ong and K. Maki, *Phys. Rev. B* **32**, 6582 (1985).
 - ⁵G. Mozurkewich and G. Grüner, *Phys. Rev. Lett.* **51**, 2206 (1983); S. E. Brown and L. Mihaly, *ibid.* **55**, 742 (1985).
 - ⁶P. Monceau, J. Richard, and M. Renard, *Phys. Rev. B* **25**, 931 (1982).
 - ⁷A. Zettl and G. Grüner, *Phys. Rev. B* **29**, 755 (1984).
 - ⁸A. Zettl and G. Grüner, *Solid State Commun.* **46**, 501 (1983).
 - ⁹S. E. Brown, G. Mozurkewich, and G. Grüner, *Phys. Rev. Lett.* **52**, 2277 (1984).
 - ¹⁰R. E. Thorne, W. G. Lyons, J. W. Lyding, and J. R. Tucker, *Phys. Rev. B* **35**, 6360 (1987).
 - ¹¹S. E. Brown, G. Mozurkewich, and G. Grüner, *Solid State Commun.* **54**, 23 (1985); S. E. Brown and G. Grüner, *Phys. Rev. B* **31**, 8302 (1985).
 - ¹²R. M. Fleming, L. F. Schneemeyer, and R. J. Cava, *Phys. Rev. B* **31**, 1181 (1985).
 - ¹³C. Schlenker, in *Low Dimensional Conductors and Superconductors*, Vol. 155 of *NATO Advanced Study Institute, Series B: Physics*, edited by D. Jérôme and L. G. Caron (Plenum, New York, 1987), p. 477.
 - ¹⁴R. J. Cava, R. M. Fleming, P. Littlewood, E. A. Rietman, L. F. Schneemeyer, and R. G. Dunn, *Phys. Rev. B* **30**, 3228 (1984).
 - ¹⁵R. P. Hall, M. S. Sherwin, and A. Zettl, *Solid State Commun.* **54**, 683 (1985).
 - ¹⁶For a review of metastable effects in $K_{0.3}MoO_3$, see R. M. Fleming in Ref. 14, p. 433.
 - ¹⁷G. Mihály, J. Dumas, and A. Jánossy, *Solid State Commun.* **60**, 785 (1986); T. W. Kim, W. P. Beyermann, B. A. Alavi, D. Reagor, and G. Grüner, *Bull. Am. Phys. Soc.* **33**, 426 (1988).
 - ¹⁸G. Grüner, A. Zawadowski, and P. M. Chaikin, *Phys. Rev. Lett.* **46**, 511 (1981).
 - ¹⁹M. F. Hundley and A. Zettl, *Solid State Commun.* **66**, 253 (1988).
 - ²⁰A. Wold, W. Kunnmann, R. J. Arnott, and A. Feretti, *Inorg. Chem.* **3**, 545 (1964).
 - ²¹J. Dumas, C. Schlenker, J. Marcus, and R. Buder, *Phys. Rev. Lett.* **50**, 757 (1983); J. Dumas and C. Schlenker, *Solid State Commun.* **45**, 885 (1983).
 - ²²A. Jánossy, G. Kriza, S. Pekker, and K. Kamarús, *Europhys. Lett.* **3**, 1027 (1987).
 - ²³G. Mihály and P. Beauchêne, *Solid State Commun.* **63**, 911 (1987).
 - ²⁴J. P. Stokes, M. O. Robbins, and S. Bhattacharya, *Bull. Am. Phys. Soc.* **30**, 214 (1985).
 - ²⁵A. Zettl and G. Grüner, *Phys. Rev. B* **28**, 2091 (1983).
 - ²⁶P. Ségransan, A. Jánossy, C. Berthier, J. Marcus, and P. Butaud, *Phys. Rev. Lett.* **56**, 1854 (1986).
 - ²⁷A. Jánossy, C. Berthier, P. Ségransan, and P. Butaud, *Phys. Rev. Lett.* **59**, 2348 (1987).
 - ²⁸G. Travaglini, P. Wachter, J. Marcus, and C. Schlenker, *Solid State Commun.* **37**, 599 (1981).
 - ²⁹M. Ganne, A. Boumaza, M. Dion, and J. Dumas, *Mater. Res. Bull.* **20**, 1297 (1985).
 - ³⁰G. H. Bouchard, Jr., J. Perlstein, and M. J. Sienko, *Inorg. Chem.* **6**, 1682 (1967); L. Forro, J. R. Cooper, A. Jánossy, and K. Kamaras, *Phys. Rev. B* **34**, 9047 (1986).
 - ³¹The magnitude of the Shapiro steps can be used to independently estimate what portion of the CDW coherently responds to the ac drive. In a simple one-dimensional model [see M. F. Hundley and A. Zettl, *Phys. Rev. B* **33**, 2883 (1986)] the relative height of the step directly yields the locked volume fraction. On the other hand, the $K_{0.3}MoO_3$ specimens studied here are more appropriately modeled as two-dimensional domain arrays. In this case, the relative Shapiro-step height is not directly proportional to the locked volume fraction. From the Shapiro-step spectrum of Fig. 3, we estimate, using a two-dimensional array model, a locked volume fraction of approximately 80% [M. F. Hundley and A. Zettl (unpublished)].
 - ³²L. Sneddon, M. C. Cross, and D. S. Fisher, *Phys. Rev. Lett.* **49**, 292 (1982).
 - ³³L. Sneddon, *Phys. Rev. Lett.* **52**, 65 (1984); *Phys. Rev. B* **29**, 719 (1984); **29**, 725 (1984).
 - ³⁴D. E. McCumber, *J. Appl. Phys.* **39**, 3113 (1968); W. C. Stewart, *Appl. Lett.* **12**, 277 (1968).
 - ³⁵H. Fack and V. Kose, *J. Appl. Phys.* **42**, 320 (1971).
 - ³⁶M. F. Hundley (unpublished).
 - ³⁷R. M. Fleming, R. J. Cava, L. F. Schneemeyer, E. A. Rietman, and R. G. Dunn, *Phys. Rev. B* **33**, 5450 (1986).
 - ³⁸J. R. Tucker, W. G. Lyons, J. H. Miller, R. E. Thorne, and J. W. Lyding, *Phys. Rev. B* **34**, 9038 (1986).
 - ³⁹P. B. Littlewood, *Phys. Rev. B* **36**, 3108 (1987).
 - ⁴⁰John Bardeen, E. Ben-Jacob, A. Zettl, and G. Grüner, *Phys. Rev. Lett.* **49**, 493 (1982).